Supporting Information

Achieving High Electrical Conductivity, Energy Storage Capacity and Cycling Stability in Ammoniated $Mo_2TiC_2T_x$ MXenes as Anode for Lithium-ion Battery

Jingya Liu, Xin Xv, Kai Wu, Hongkang Wang, Pengfei Wang, Yonghong Cheng*, Bing Xiao*
School of Electrical Engineering, Xi'an Jiaotong University, Xi'an Shaanxi, 710049, P.R. China
Corresponding authors: cyh@xjtu.edu.cn; bingxiao84@xjtu.edu.cn

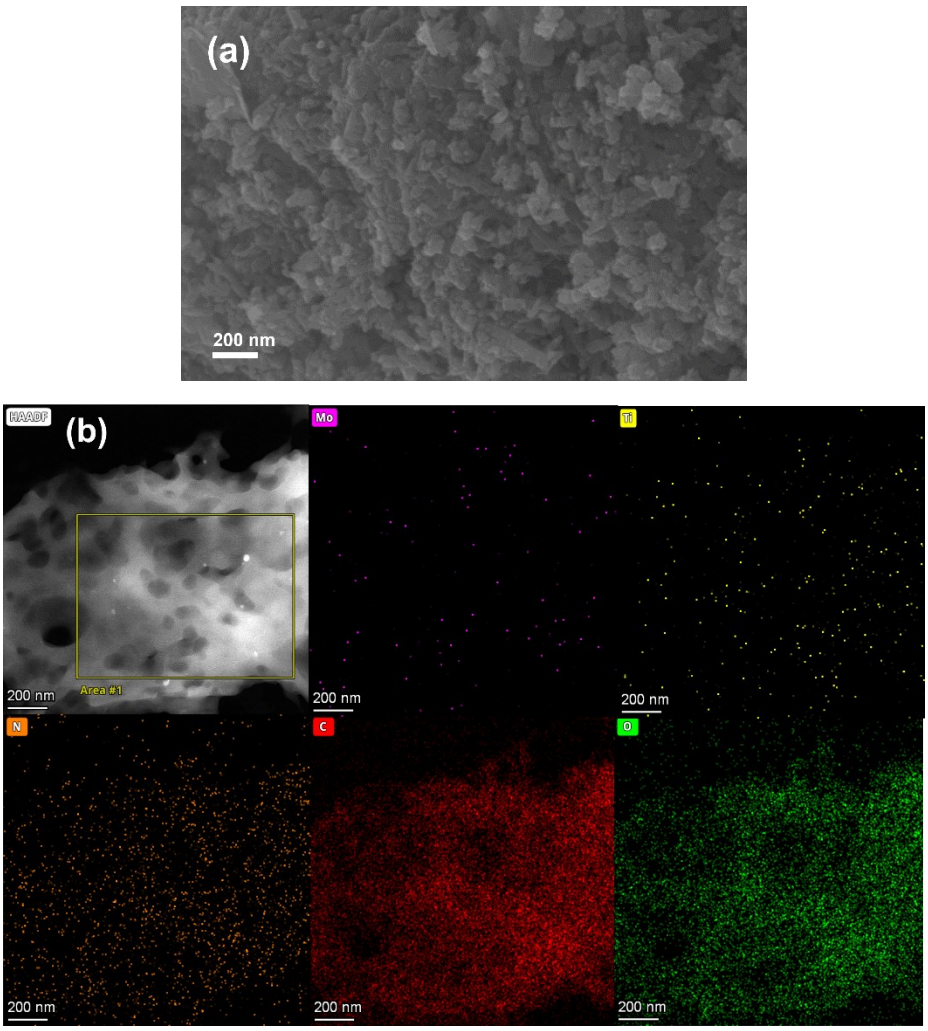

Figure S1. (a) The SEM image of Mo_2TiC_2-N600-2h; (b) the HAADF image and the EDS mapping images of $Mo_2TiC_2T_x$-N600-2h.

Table S1. The element component fraction from EDS in Fig. S1(b)

Element	Atomic Fraction (%)	Mass Fraction (%)
C	86.74	82.87
N	0.4	0.44
O	12.81	16.3
Ti	0.02	0.06
Mo	0.04	0.33

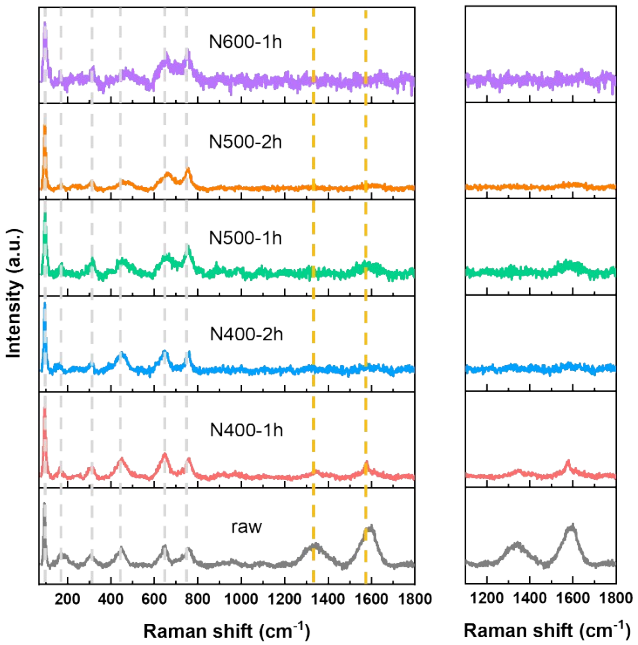

Figure S2. Raman spectra of Mo_2TiC_2 before and after ammoniation at 400, 500 and 600 ℃ for 1h/2h and then 300 ℃ annealing in N_2 for 1h. All spectra were collected with a 532 nm laser after 30s of exposure to 10% power.

The two peaks within the wavenumber range of 1300~1600 cm^{-1} (1342.9 and 1598.7 cm^{-1}) are distinctive Raman features at around 1355 (D peak) and 1600 cm^{-1} (G peak) of graphene, which means the SP2 hybridized peak commonly presented in transition metal carbides (TMDs)[1]. After ammonification at 400, 500 and 600℃, the peaks of carbon vibrations region nearly disappear, indicated that the hybrid structure of SP2 has undergone a change, with nitrogen elements added to the graphite structure, which disrupts its symmetry.

The layer size (L_c) was estimated using the Scherrer equation (Eqs. 1)[2]:

$$L_c = A\lambda/(B\cos\theta) \quad (1)$$

where A is the shape factor (~0.943); λ is the X-ray wavelength (~1.54056 Å); θ the Bragg angle; B is the full width at half maximum (FWHM) of the (002) peak in radians. The results are listed in main article Table 1. The crystallite size decreased slightly on introduction of ammoniation at 400 °C from 1 h to 2 h. However, the decrease in L_c becomes more significant by increasing the temperature up to 500 °C. L_c is based on the (002) peak and reflects the Z dimension of the MXenes plates (thickness)[3][4]; the parameters are listed in main article Table 1. When the ammoniation temperature exceeded 500 °C, the L_c was nearly reduced to half.

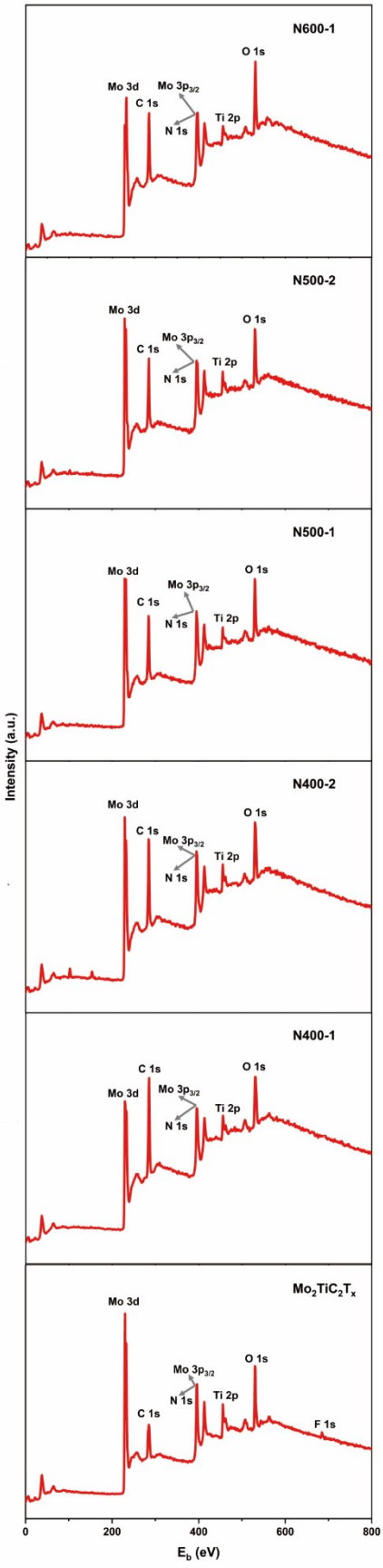

Figure S3. XPS spectra of N-600, 500, 400 and $Mo_2TiC_2T_x$ respectively.

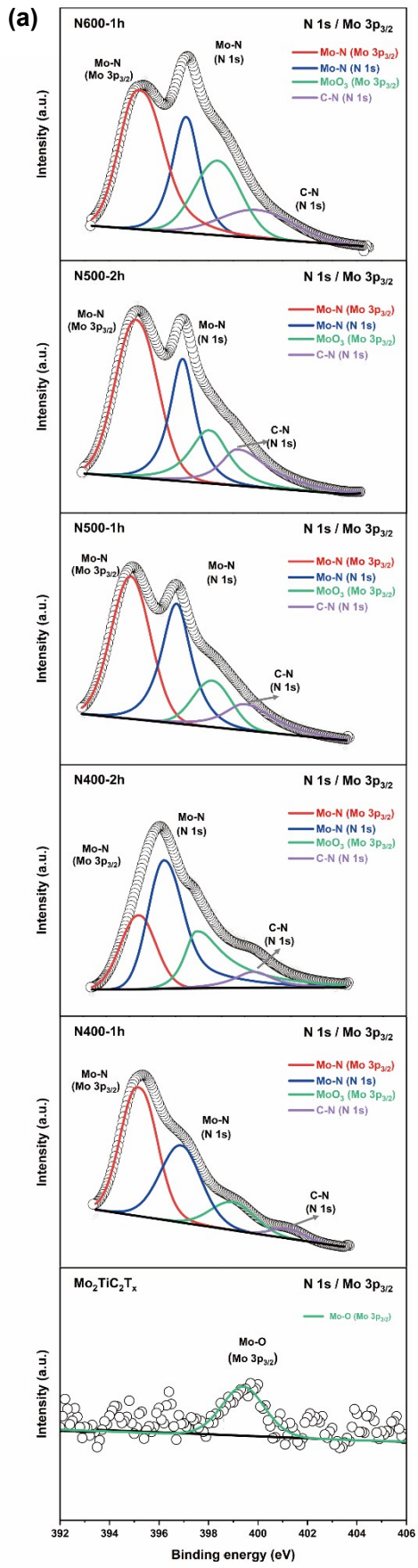
(a)
N600-1h
N 1s / Mo 3p3/2
Mo-N (Mo 3p3/2)
Mo-N (N 1s)
MoO3 (Mo 3p3/2)
C-N (N 1s)
Mo-N (Mo 3p3/2)
Mo-N (N 1s)
C-N (N 1s)
Intensity (a.u.)
N500-2h
N 1s / Mo 3p3/2
Mo-N (Mo 3p3/2)
Mo-N (N 1s)
MoO3 (Mo 3p3/2)
C-N (N 1s)
Mo-N (Mo 3p3/2)
Mo-N (N 1s)
C-N (N 1s)
Intensity (a.u.)
N500-1h
N 1s / Mo 3p3/2
Mo-N (Mo 3p3/2)
Mo-N (N 1s)
MoO3 (Mo 3p3/2)
C-N (N 1s)
Mo-N (Mo 3p3/2)
Mo-N (N 1s)
C-N (N 1s)
Intensity (a.u.)
N400-2h
N 1s / Mo 3p3/2
Mo-N (Mo 3p3/2)
Mo-N (N 1s)
MoO3 (Mo 3p3/2)
C-N (N 1s)
Mo-N (N 1s)
Mo-N (Mo 3p3/2)
C-N (N 1s)
Intensity (a.u.)
N400-1h
N 1s / Mo 3p3/2
Mo-N (Mo 3p3/2)
Mo-N (N 1s)
MoO3 (Mo 3p3/2)
C-N (N 1s)
Mo-N (Mo 3p3/2)
Mo-N (N 1s)
C-N (N 1s)
Intensity (a.u.)
Mo2TiC2Tx
N 1s / Mo 3p3/2
Mo-O (Mo 3p3/2)
Mo-O (Mo 3p3/2)
Intensity (a.u.)
392
394
396
398
400
402
404
406
Binding energy (eV)

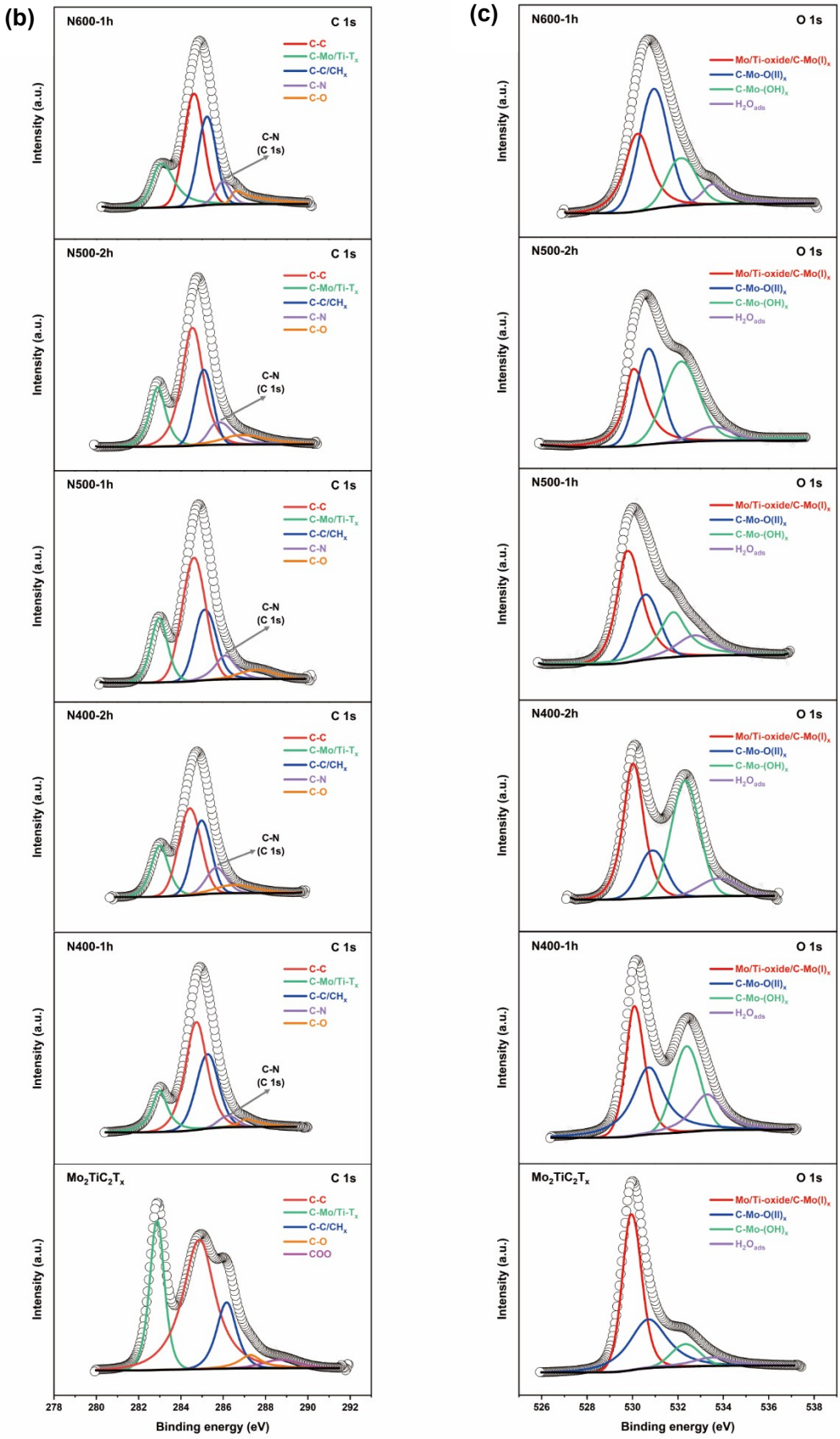
(b)
N600-1h
C 1s
C-C
C-Mo/Ti-Tx
C-C/CHx
C-N
C-O
C-N
(C 1s)
N500-2h
C 1s
N500-1h
C 1s
N400-2h
C 1s
N400-1h
C 1s
Mo2TiC2Tx
C 1s
C-C
C-Mo/Ti-Tx
C-C/CHx
C-O
COO
Intensity (a.u.)
278
280
282
284
286
288
290
292
Binding energy (eV)
(c)
N600-1h
O 1s
Mo/Ti-oxide/C-Mo(I)x
C-Mo-O(II)x
C-Mo-(OH)x
H2Oads
N500-2h
O 1s
N500-1h
O 1s
N400-2h
O 1s
N400-1h
O 1s
Mo2TiC2Tx
O 1s
Intensity (a.u.)
526
528
530
532
534
536
538
Binding energy (eV)

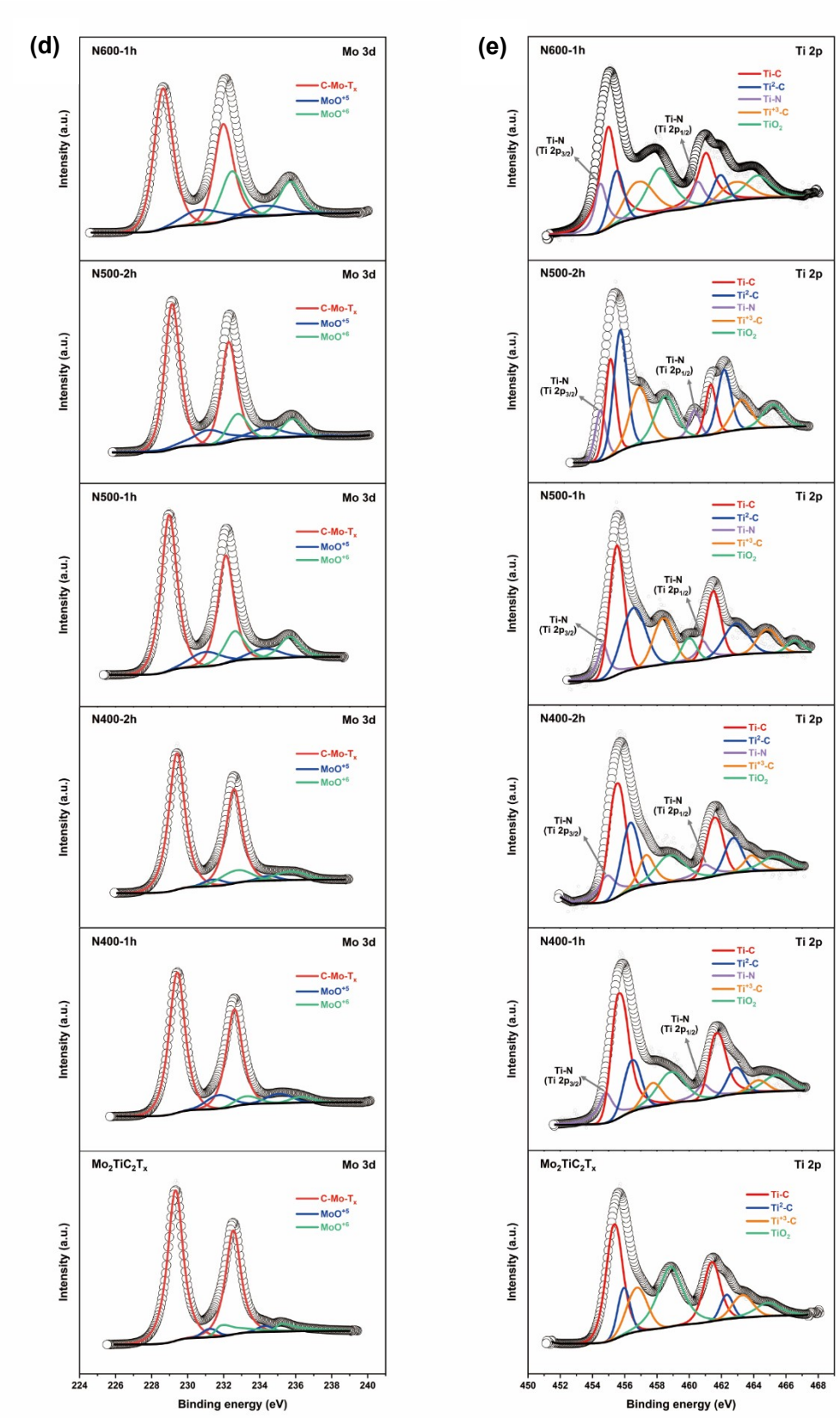

Figure S4. High-resolution XPS spectra deconvolution of (a) N 1s, (b) C 1s, (c) O 1s, (d) Mo 3d and (e) Ti 2p region for N-600, 500, 400 and $Mo_2TiC_2T_x$ respectively.

Table S2. Summary of global atomic compositions of the high resolution XPS region fittings of $Mo_2TiC_2T_x$

Region	Be[eV]	FWHM[eV]	Atomic %	Weight %	Assigned to	Reference
C1s	282.85	0.82	9.5	2.88	C-Mo/Ti-T_x	[5]
	284.84	1.8	19.8	6	C-C	[5]
	286.16	1.11	5.71	1.73	C-C/CH_x	[5]
	287.28	1.23	1.44	0.44	C-O	[7]
	288.68	2.04	1.26	0.38	COO	[5]
Mo3d	229.31	1.01	12.28	29.73	C-Mo-T_x	[6]
	232.53	1.01	12.3	29.76		
	231.24	0.99	0.58	1.4	MoO^{+5}	[5]
	234.29	0.99	0.58	1.4		
	231.88	1.36	1.34	3.25	MoO^{+6}	[5]
	235.23	1.36	1.34	3.25		
O1s	529.93	1.01	9.82	3.97	Mo/Ti-oxide/C-Mo$(I)_x$	[5]
	530.7	1.98	6.62	2.67	C-Mo-$O(II)_x$	[5]
	532.34	1.49	1.99	0.8	C-Mo-$(OH)_x$	[5]
	533.49	2	1.29	0.52	H_2O_{ads}	[5]
Ti2p	455.33	1.23	2.16	2.98	Ti-C	[5]
	461.38	1.23	2.4	3.32		
	455.95	0.9	0.62	0.86	Ti^2-C	[5]
	462.32	0.9	0.69	0.95		
	456.76	1.5	0.96	1.32	Ti^{+3}-C	[5]
	463.31	1.5	1.06	1.47		
	458.82	1.83	1.75	2.43	TiO_2	[5]
	464.87	1.83	0.84	1.17		

Table S3. Summary of global atomic compositions of the high resolution XPS region fittings of N600-1h

Region	Be[eV]	FWHM[eV]	Atomic %	Weight %	Assigned to	Reference
C1s	283.02	1.27	6.84	2.64	C-Mo/Ti-T_x	[5]
	284.6	1.12	13.84	5.34	C-C	[5]
	285.23	1.01	9.75	3.76	C-C/CH_x	[5]
	285.98	0.83	2.16	0.83	C-N	[7]
	286.58	1.24	2.34	0.9	C-O	[5]
Mo3d	229.35	1.17	6	18.49	C-Mo-T_x	[6]
	232.5	1.17	6	18.5		
	231.24	2.36	1.23	3.78	MoO^{+5}	[5]
	234.59	2.36	1.23	3.79		
	232.95	1.32	2.24	6.9	MoO^{+6}	[5]
	236	1.32	2.24	6.9		
N1s/Mo3$p_{3/2}$	395.14	2.1	10.59	4.77	Mo-N (Mo 3$p_{3/2}$)	[6]
	397.08	1.3	5.69	2.56	Mo-N (N1s)	[6]
	398.37	2.22	5.72	2.58	MoO_3 (Mo 3$p_{3/2}$)	[6]
	399.95	3.5	3.43	1.54	C-N (N 1s)	[7]
O1s	530.2	1.38	4.37	2.24	Mo/Ti-oxide/C-Mo(I)$_x$	[5]
	530.94	1.52	6.5	3.34	C-Mo-O(II)$_x$	[5]
	532.09	1.56	2.67	1.38	C-Mo-(OH)$_x$	[5]
	533.52	1.3	1.25	0.64	H_2O_{ads}	[5]
Ti2p	454.45	0.87	0.34	0.53	Ti-N	[7]
	460.5	0.87	0.38	0.59		
	454.98	1.23	1.01	1.55	Ti-C	[5]
	461.03	1.23	1.12	1.73		
	455.49	1.05	0.35	0.54	Ti^2-C	[5]
	461.93	1.05	0.39	0.6		
	456.76	2.12	0.5	0.77	Ti^{+3}-C	[5]
	462.81	2.12	0.55	0.85		
	458.17	1.93	0.6	0.92	TiO_2	[5]
	464.22	1.93	0.67	1.03		

Table S4. Summary of global atomic compositions of the high resolution XPS region fittings of N500-1h

Region	Be[eV]	FWHM[eV]	Atomic %	Weight %	Assigned to	Reference
C1s	282.97	0.94	6.37	2.4	C-Mo/Ti-T_x	[5]
	284.61	1.32	16.5	6.22	C-C	[5]
	285.10	1.21	8.81	3.32	C-C/CH_x	[5]
	286.09	1.14	3.05	1.15	C-N	[7]
	287.59	2	1.85	0.7	C-O	[5]
Mo3d	228.96	1.04	7.03	21.17	C-Mo-T_x	[6]
	232.11	1.04	7.04	21.19		
	231.01	2	1.13	3.41	MoO^{+5}	[5]
	234.29	2	1.13	3.41		
	232.61	1.34	1.7	5.12	MoO^{+6}	[5]
	235.66	1.34	1.7	5.12		
N1s/Mo3$p_{3/2}$	394.86	1.86	10.63	4.67	Mo-N (Mo 3$p_{3/2}$)	[6]
	396.7	1.42	7.8	3.43	Mo-N (N1s)	[6]
	398.15	1.82	3.4	1.49	MoO_3 (Mo 3$p_{3/2}$)	[6]
	399.44	2.33	2.84	1.25	C-N (N 1s)	[7]
O1s	529.75	1.3	5.7	2.86	Mo/Ti-oxide/C-Mo(I)$_x$	[5]
	530.57	1.42	3.28	1.65	C-Mo-O(II)$_x$	[5]
	531.79	1.48	3.12	1.56	C-Mo-(OH)$_x$	[5]
	532.75	1.93	1.54	0.77	H_2O_{ads}	[5]
Ti2p	454.65	0.8	0.31	0.48	Ti-N	[7]
	460.85	0.8	0.35	0.53		
	455.51	1.09	1.14	1.71	Ti-C	[5]
	461.49	1.09	1.26	1.9		
	456.55	1.74	0.86	1.3	Ti^2-C	[5]
	462.91	1.74	0.96	1.44		
	458.36	1.48	0.55	0.83	Ti^{+3}-C	[5]
	464.81	1.48	0.6	0.91		
	459.97	1.07	0.2	0.3	TiO_2	[5]
	466.52	1.07	0.22	0.33		

Table S5. Summary of global atomic compositions of the high resolution XPS region fittings of N400-1h

Region	Be[eV]	FWHM[eV]	Atomic %	Weight %	Assigned to	Reference
C1s	282.99	0.90	7.16	2.97	C-Mo/Ti-T_x	[5]
	284.63	1.16	20.92	8.69	C-C	[5]
	285.16	1.07	14.31	5.94	C-C/CH_x	[5]
	286.03	1.2	3.74	1.55	C-N	[7]
	287.03	0.95	1.1	0.46	C-O	[5]
Mo3d	229.41	1.05	6.79	22.53	C-Mo-T_x	[6]
	232.58	1.05	6.8	22.55		
	231.70	1.63	0.85	2.84	MoO^{+5}	[5]
	235.05	1.63	0.86	2.84		
	233.21	1.65	0.59	1.95	MoO^{+6}	[5]
	236.26	1.65	0.59	1.95		
N1s/Mo3$p_{3/2}$	394.56	1.16	3.26	1.58	Mo-N (Mo 3$p_{3/2}$)	[6]
	395.45	1.17	4.75	2.3	Mo-N (N1s)	[6]
	396.68	1.84	5.87	2.84	MoO_3 (Mo 3$p_{3/2}$)	[6]
	398.59	3.42	3.88	1.88	C-N (N 1s)	[7]
O1s	530.02	1.02	4.88	2.70	Mo/Ti-oxide/C-Mo(I)$_x$	[5]
	530.56	1.23	2.12	1.17	C-Mo-O(II)$_x$	[5]
	532.35	1.56	3.98	2.21	C-Mo-(OH)$_x$	[5]
	533.23	1.93	2.20	1.22	H_2O_{ads}	[5]
Ti2p	454.82	1.1	0.34	0.57	Ti-N	[7]
	460.87	1.1	0.39	0.64		
	455.62	1.27	1.31	2.17	Ti-C	[5]
	461.67	1.27	1.46	2.42		
	456.44	1.26	0.5	0.83	Ti^2-C	[5]
	462.88	1.26	0.56	0.93		
	457.74	1.33	0.24	0.4	Ti^{+3}-C	[5]
	464.29	1.33	0.27	0.45		
	458.83	2.02	0.51	0.85	TiO_2	[5]
	465.38	2.02	0.57	0.95		

Table S6. Summary of global atomic compositions of the high resolution XPS region fittings of N500-2h

Region	Be[eV]	FWHM[eV]	Atomic %	Weight %	Assigned to	Reference
C1s	282.9	0.89	6.27	2.28	C-Mo/Ti-T_x	[5]
	284.52	1.21	16.52	6.01	C-C	[5]
	285.08	1	7.95	2.89	C-C/CH_x	[5]
	285.74	1.28	3.36	1.22	C-N	[7]
	286.77	2.47	2.81	1.02	C-O	[5]
Mo3d	229.12	1.02	6.87	20	C-Mo-T_x	[6]
	232.27	1.02	6.88	20.02		
	231.12	2.18	1.78	5.17	MoO^{+5}	[5]
	234.33	2.18	1.78	5.19		
	232.77	1.29	1.46	4.23	MoO^{+6}	[5]
	235.82	1.29	1.46	4.24		
N1s/Mo3$p_{3/2}$	395.04	2.01	12.31	5.23	Mo-N (Mo 3$p_{3/2}$)	[6]
	396.95	1.22	6.75	2.87	Mo-N (N1s)	[6]
	397.99	1.84	4.39	1.86	MoO_3 (Mo 3$p_{3/2}$)	[6]
	399.14	2.28	3.86	1.64	C-N (N 1s)	[7]
O1s	530.03	1.15	3.85	1.87	Mo/Ti-oxide/C-Mo(I)$_x$	[5]
	530.72	1.32	4.6	2.23	C-Mo-O(II)$_x$	[5]
	532.15	1.83	6.02	2.92	C-Mo-(OH)$_x$	[5]
	533.53	1.97	1.09	0.53	H_2O_{ads}	[5]
Ti2p	455.02	0.7	0.27	0.42	Ti-N	[7]
	460.24	0.7	0.3	0.47		
	455.57	0.7	0.53	0.81	Ti-C	[5]
	461.14	0.7	0.59	0.9		
	456.12	0.88	0.83	1.27	Ti^2-C	[5]
	461.89	0.88	0.92	1.41		
	457.18	1.25	0.55	0.85	Ti^{+3}-C	[5]
	462.84	1.25	0.61	0.94		
	458.62	1.37	0.46	0.71	TiO_2	[5]
	464.6	1.37	0.52	0.79		

Table S7. Summary of global atomic compositions of the high resolution XPS region fittings of N400-2h

Region	Be[eV]	FWHM[eV]	Atomic %	Weight %	Assigned to	Reference
C1s	283	0.97	7.42	2.91	C-Mo/Ti-T_x	[5]
	284.41	1.24	15.2	5.95	C-C	[5]
	284.97	1.07	11.11	4.35	C-C/CH_x	[5]
	285.66	1.13	4.18	1.64	C-N	[7]
	286.41	2.24	2.74	1.07	C-O	[5]
Mo3d	229.39	1.05	7.26	22.72	C-Mo-T_x	[6]
	232.56	1.05	7.27	22.75		
	231.4	1.29	0.36	1.17	MoO^{+5}	[5]
	234.45	1.29	0.36	1.17		
	232.64	2.02	1.14	3.57	MoO^{+6}	[5]
	235.69	2.02	1.14	3.56		
N1s/$Mo3p_{3/2}$	394.38	1.81	5.82	3.02	Mo-N (Mo $3p_{3/2}$)	[6]
	395.5	1.81	11.69	5.34	Mo-N (N1s)	[6]
	396.91	2.08	6.57	3	MoO_3 (Mo $3p_{3/2}$)	[6]
	399.38	1.97	1.62	0.74	C-N (N 1s)	[7]
O1s	530	1.07	5.32	2.77	Mo/Ti-oxide/C-Mo$(I)_x$	[5]
	530.86	1.41	2.25	1.17	C-Mo-$O(II)_x$	[5]
	532.32	1.46	5.69	2.97	C-Mo-$(OH)_x$	[5]
	533.82	2	1.18	0.62	H_2O_{ads}	[5]
Ti2p	454.9	1.3	0.34	0.56	Ti-N	[7]
	460.95	1.3	0.38	0.62		
	455.5	1.23	1.08	1.77	Ti-C	[5]
	461.55	1.23	1.2	1.97		
	456.35	1.26	0.66	1.08	Ti^2-C	[5]
	462.73	1.26	0.73	1.2		
	457.32	1.16	0.3	0.49	Ti^{+3}-C	[5]
	463.85	1.16	0.34	0.55		
	458.71	2	0.47	0.78	TiO_2	[5]
	465.26	2	0.53	0.86		

Table S8. The Hall effect and electrical properties of Mo_2TiC_2

Tempe-rature (K)	Conduc-tivity type	Carrier areal density (cm^{-2})	Carrier volume density (cm^{-3})	Resistivity (Ω·cm)	Hall coefficient (cm^3/C)	Carrier mobility (cm^2/Vs)
100	n	2.20948E18	1.82601E21	0.00194	-0.00342	1.76312
200	n	2.36775E18	1.95682E21	0.00239	-0.00319	1.33514
300	n	2.50084E18	2.06681E21	0.00298	-0.00302	1.01376
400	n	2.71187E18	2.24122E21	0.00368	-0.00278	0.75651

Table S9. The Hall effect and electrical properties of Mo_2TiC_2-N400-1h

Tempe-rature (K)	Conduc-tivity type	Carrier areal density (cm^{-2})	Carrier volume density (cm^{-3})	Resistivity (Ω·cm)	Hall coefficient (cm^3/C)	Carrier mobility (cm^2/Vs)
100	n	1.66662E19	5.41752E21	0.00113	-0.00277	2.03618
200	n	1.63014E19	5.29898E21	0.00139	-0.00284	1.69532
300	n	1.64414E19	5.34449E21	0.00174	-0.00281	1.34295
400	n	1.73994E19	5.6559E21	0.00214	-0.00266	1.03546

Table S10. The Hall effect and electrical properties of Mo_2TiC_2- N500-1h

Tempe-rature (K)	Conduc-tivity type	Carrier areal density (cm^{-2})	Carrier volume density (cm^{-3})	Resistivity (Ω·cm)	Hall coefficient (cm^3/C)	Carrier mobility (cm^2/Vs)
100	n	1.90015E19	5.56818E21	9.44444E-4	-0.00173	1.35142
200	n	1.90558E19	5.58412E21	0.00116	-0.00172	1.08764
300	n	2.23638E19	6.55348E21	0.00145	-0.00147	0.76458
400	n	3.04281E19	8.91665E21	0.00178	-0.00108	0.49373

Table S11. The Hall effect and electrical properties of Mo_2TiC_2- N600-1h

Tempe-rature (K)	Conduc-tivity type	Carrier areal density (cm^{-2})	Carrier volume density (cm^{-3})	Resistivity (Ω·cm)	Hall coefficient (cm^3/C)	Carrier mobility (cm^2/Vs)
100	n	1.50392E19	6.65453E21	7.99364E-4	-9.37707E-4	1.17307
200	n	1.81028E19	8.01009E21	9.45035E-4	-7.79017E-4	0.82433
300	n	2.21135E19	9.78474E21	0.00111	-6.37728E-4	0.57682
400	n	2.82886E19	1.25171E22	0.00126	-4.98519E-4	0.39576

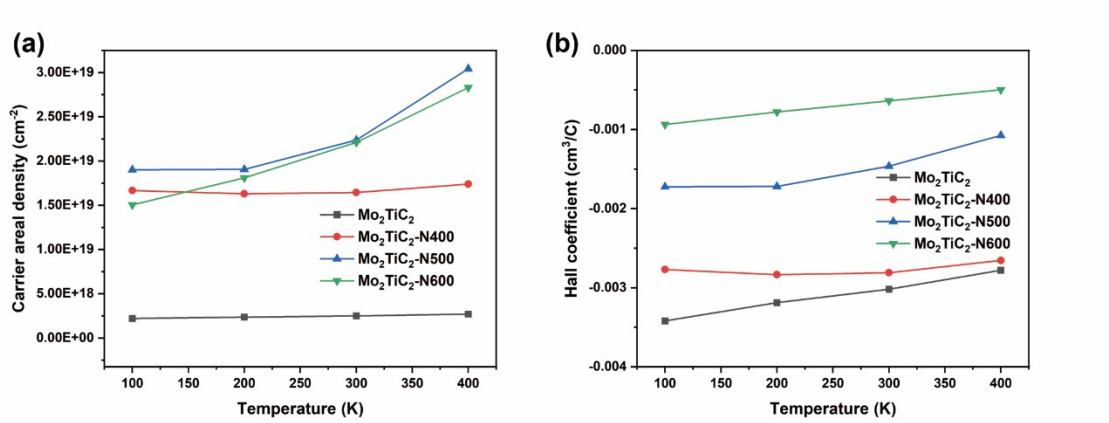

Figure S5. (a) Carrier areal density and (b) Hall coefficient and of Mo_2TiC_2, Mo_2TiC_2-N400-1h, Mo_2TiC_2-N500-1h and Mo_2TiC_2-N600-1h.

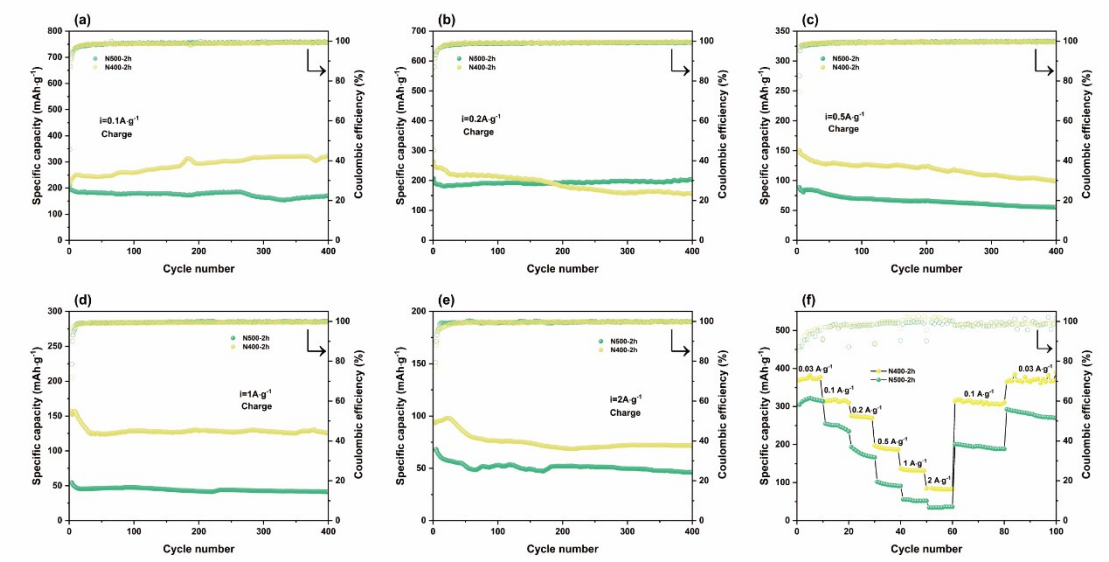

Figure S6. Cycling performances of $Mo_2TiC_2T_x$ and N400/500-2h at (a) 0.1 A·g^{-1}, (b) 0.2 A·g^{-1}, (c) 0.5 A·g^{-1}, (d) 1 A·g^{-1} and (e) 2 A·g^{-1}. (f) Rate capability testing at 0.1, 0.2, 0.5, 1, 2 A·g^{-1} for 10 cycles at each rate for N400/500-2h samples.

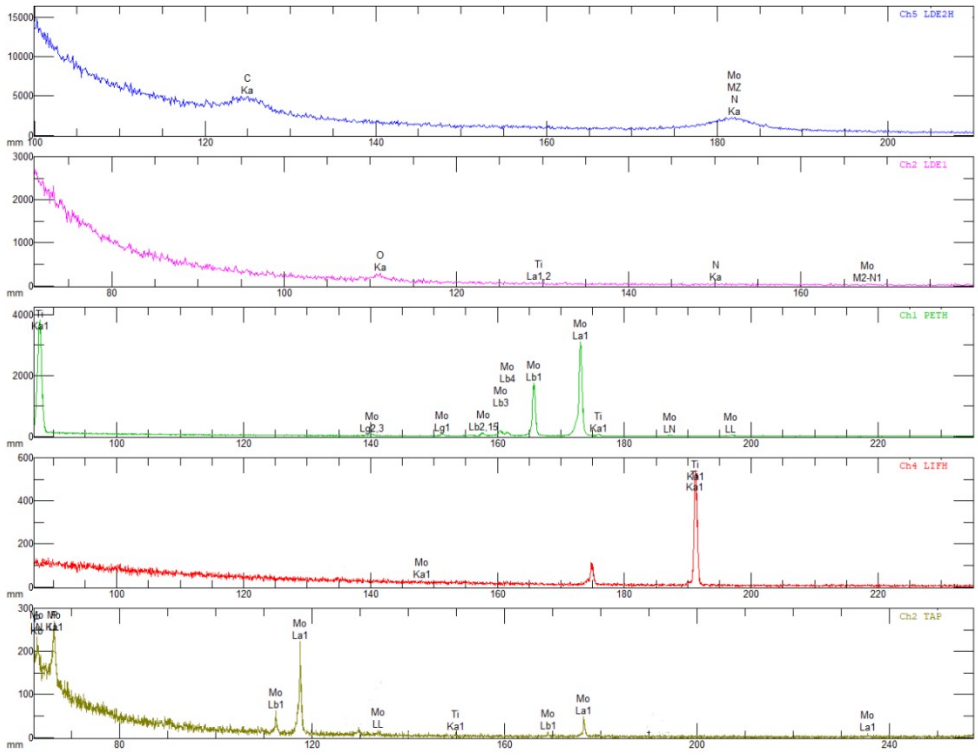

(a)

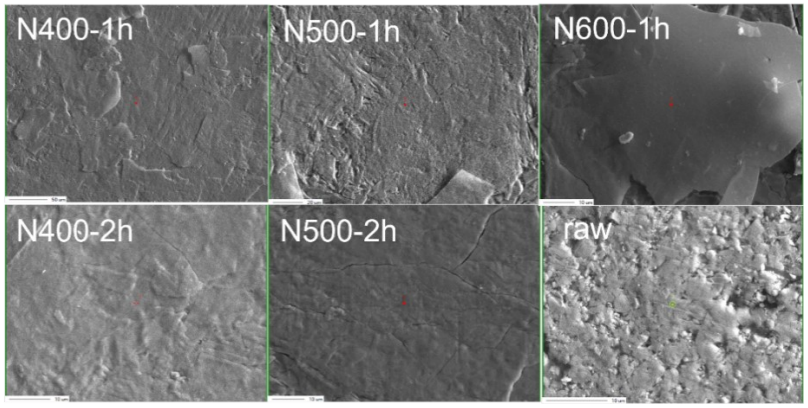

(b)

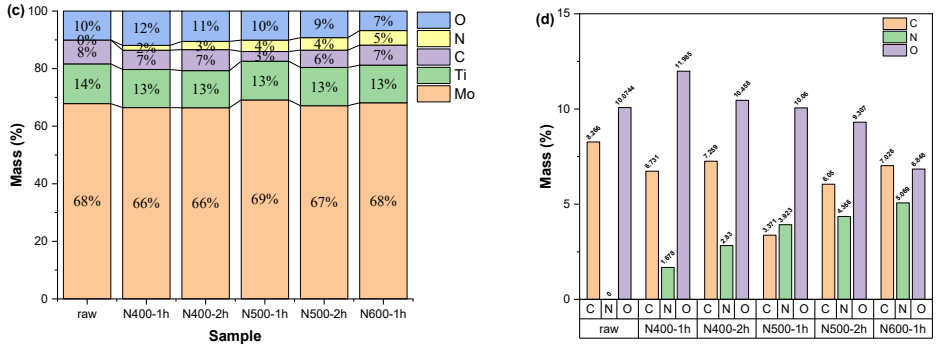

Figure S7. (a) The spectrum of N400-1h. (b) The carbon, nitrogen and oxygen atomic fraction of all samples. (c) The all-element mass fraction of all samples. (d) The carbon, nitrogen and oxygen mass fraction of all samples.

Table S12. Summary of global atomic compositions of the high resolution XPS region fittings of N400-1h at 0.01 V

Region	Be[eV]	FWHM[eV]	Atomic %	Weight %	Assigned to	Reference
C1s	284.8	1.45	8.58	7.31	C-C/CH_x	[5]
	286.53	1.34	0.97	0.83	C-O	[5]
	288.47	1.77	3.29	2.8	C-OO	[7]
	289.78	1.23	9.56	8.15	CO_3	[9]
Mo3d	231.1	1.96	0.15	0.99	MoO^{+4}/$Mo(OH)_x$	[10]
	234.15	1.96	0.15	1		
	232.51	1.08	0.91	6.19	MoO^{+5}	[5]
	235.65	1.08	0.88	5.97		
	232.9	1.31	0.08	0.55	MoO^{+6}	[5]
	236.06	1.31	0.08	0.55		
N1s/$Mo3p_{3/2}$	394.39	2.08	0.17	0.17	Mo-N (Mo $3p_{3/2}$)	[6]
	396.32	2.06	0.58	0.58	Mo/Ti-N (N1s)	[6]
	398.15	2.04	2.31	2.3	MoO_3 (Mo $3p_{3/2}$)	[6]
	399.62	2.24	0.84	0.83	C-N (N 1s)	[7]
O1s	530.45	1.23	5.4	6.13	Li_2O/Mo/Ti-oxide	[11]
	531.48	0.94	11.87	13.47	LiOH/C-Mo-O(II)$_x$	[12]
	532.04	1.38	24.14	27.39	Li_2CO_3/C-Mo-$(OH)_x$	[9]
Li1s	54.13	1.67	2.98	1.46	Li_2O	[11]
	54.83	1.02	7.6	3.74	LiOH	[12]
	55.4	1.33	19.46	9.58	Li_2CO_3	[9]

Table S13. Summary of global atomic compositions of the high resolution XPS region fittings of N400-1h at 1.39 V

Region	Be[eV]	FWHM[eV]	Atomic %	Weight %	Assigned to	Reference
C1s	284.8	1.44	8.79	7.51	C-C/CH_x	[5]
	286.64	1.04	0.45	0.38	C-O	[5]
	288.71	1.76	3.86	3.3	C-OO	[7]
	289.86	1.21	8.96	7.66	CO_3	[9]
Mo3d	231.1	2.12	0.11	0.77	MoO^{+4}/$Mo(OH)_x$	[10]
	234.15	2.12	0.11	0.77		
	232.51	1	0.71	4.88	MoO^{+5}	[5]
	235.64	1	0.72	4.89		
	232.9	0.86	0.29	1.96	MoO^{+6}	[5]
	236.06	0.86	0.29	1.96		
N1s/$Mo3p_{3/2}$	394.46	3.12	0.36	0.36	Mo-N (Mo $3p_{3/2}$)	[6]
	396.43	1.95	0.52	0.51	Mo/Ti-N (N1s)	[6]
	398.26	2.15	2.57	2.56	MoO_3 (Mo $3p_{3/2}$)	[6]
	400.15	1.96	0.57	0.57	C-N (N 1s)	[7]
O1s	530.3	1.29	4.43	5.04	Li_2O/Mo/Ti-oxide	[11]
	531.43	1.14	14.52	16.54	LiOH/C-Mo-O(II)$_x$	[12]
	532.03	1.31	22.1	25.18	Li_2CO_3/C-Mo-$(OH)_x$	[9]
Li1s	54.13	1.34	1.72	0.85	Li_2O	[11]
	54.83	1.02	9.59	4.74	LiOH	[12]
	55.4	1.25	19.33	9.55	Li_2CO_3	[9]

Table S14. Summary of global atomic compositions of the high resolution XPS region fittings of N400-1h at 3 V

Region	Be[eV]	FWHM[eV]	Atomic %	Weight %	Assigned to	Reference
C1s	284.8	1.35	10.68	10.23	C-C/CH_x	[5]
	286.41	1.49	1.07	1.02	C-O	[5]
	288.59	1.52	4.12	3.95	C-OO	[7]
	289.83	1.23	10.08	9.65	CO_3	[9]
Mo3d	228.57	1.92	0.01	0.04	M-O	[13]
	229.73	1.81	0.04	0.33	C/N-Mo-T_x	[6][14]
	232.55	1.8	0.04	0.33		
	231.1	1.82	0.03	0.22	MoO^{+4}/$Mo(OH)_x$	[10]
	234.21	1.82	0.03	0.22		
	232.52	1.22	0.1	0.76	MoO^{+5}	[5]
	235.63	1.22	0.1	0.76		
	232.91	1.08	0.09	0.71	MoO^{+6}	[5]
	236.06	1.08	0.09	0.71		
N1s/$Mo3p_{3/2}$	393.7	2	0.07	0.08	Mo-N (Mo $3p_{3/2}$)	[6]
	395.97	2.87	0.32	0.35	Mo/Ti-N (N1s)	[6]
	398.21	2	0.43	0.48	MoO_3 (Mo $3p_{3/2}$)	[6]
	399.81	2	0.22	0.24	C-N (N 1s)	[7]
O1s	530.32	1.63	3.08	3.93	Li_2O/Mo/Ti-oxide	[11]
	531.36	1.09	15.86	20.23	LiOH/C-Mo-O(II)$_x$	[12]
	531.94	1.3	22.34	28.49	Li_2CO_3/C-Mo-$(OH)_x$	[9]
Li1s	54.08	1.67	1.72	0.95	Li_2O	[11]
	54.79	1.03	8.87	4.91	LiOH	[12]
	55.41	1.25	20.59	11.39	Li_2CO_3	[9]

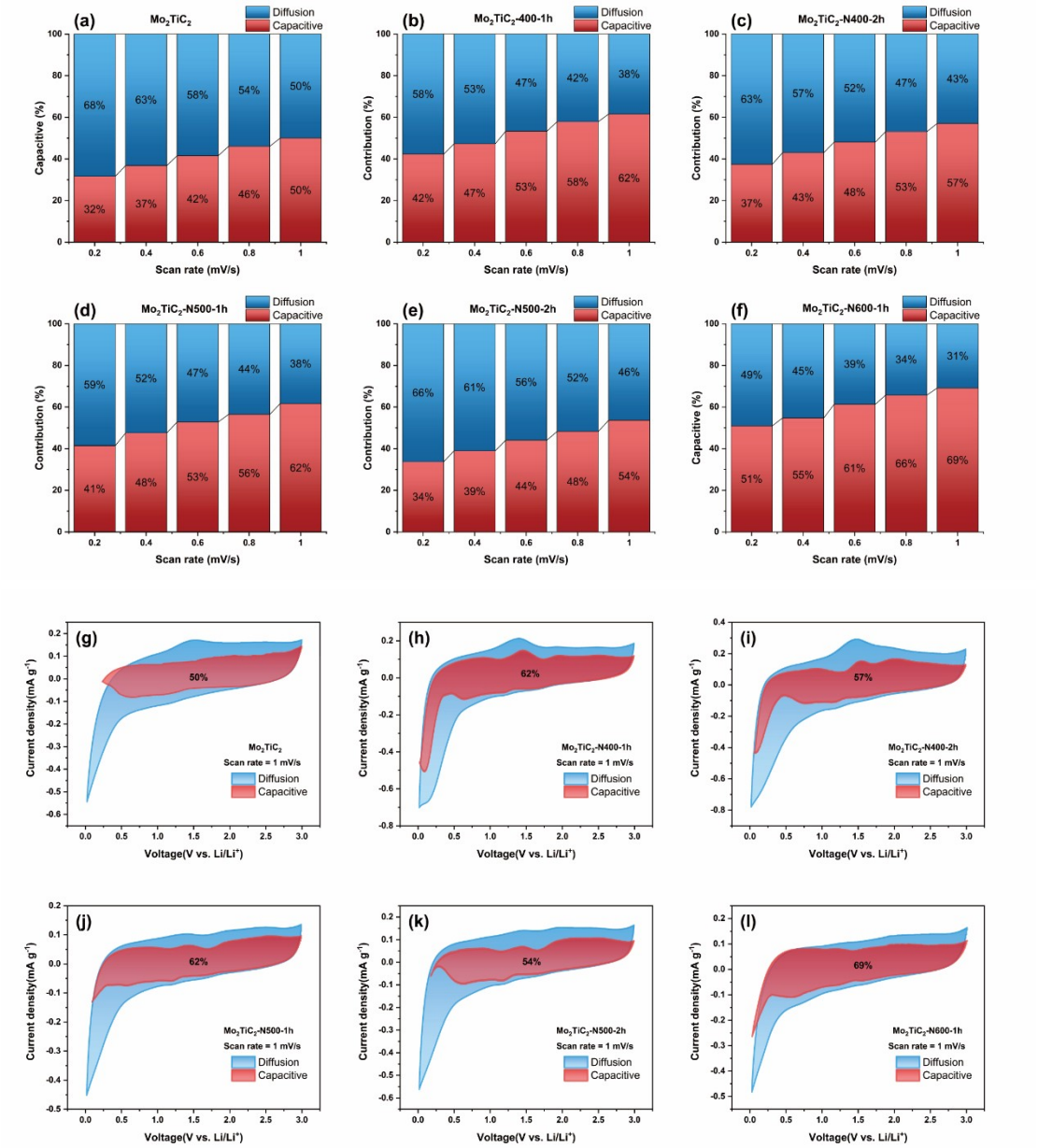

Figure S8. Pseudocapacitive and diffusion-controlled capacity contribution ratio for sample (a)(g) raw, (b)(h) N400-1h, (c)(i) N400-2h, (d)(j) N500-1h, (e)(k) N500-2h and (f)(l) N600-1h.

The pseudocapacitive contributions at different scan rates can be calculated by the equations described as below[8]:

$$i = k_1 v + k_2 v^{1/2} \tag{1}$$

$$i v^{-1/2} = k_1 v^{1/2} + k_2 \tag{2}$$

where k_1 and k_2 are constants for a given potential. Fig. S4 displays the calculated contribution ratios of two capacity mechanism at different scan rates ranging from 0.2 to 1.0 mVs^{-1}. As the scan rates increase, the capacity contribution ratios of all samples gradually raise. Actually, all

samples are mainly controlled by the Faradic process. The larger capacitive charge storage can be responsible for the high-rate capability of $Mo_2TiC_2T_x$. A shaded region related to the surface-controlled capacity contributions is illustrated at the scan rate of 0.2 mVs^{-1}, comprising about 46% of the total capacity. Compare to the raw $Mo_2TiC_2T_x$, the capacity contribution ratios of nitride samples are all higher.

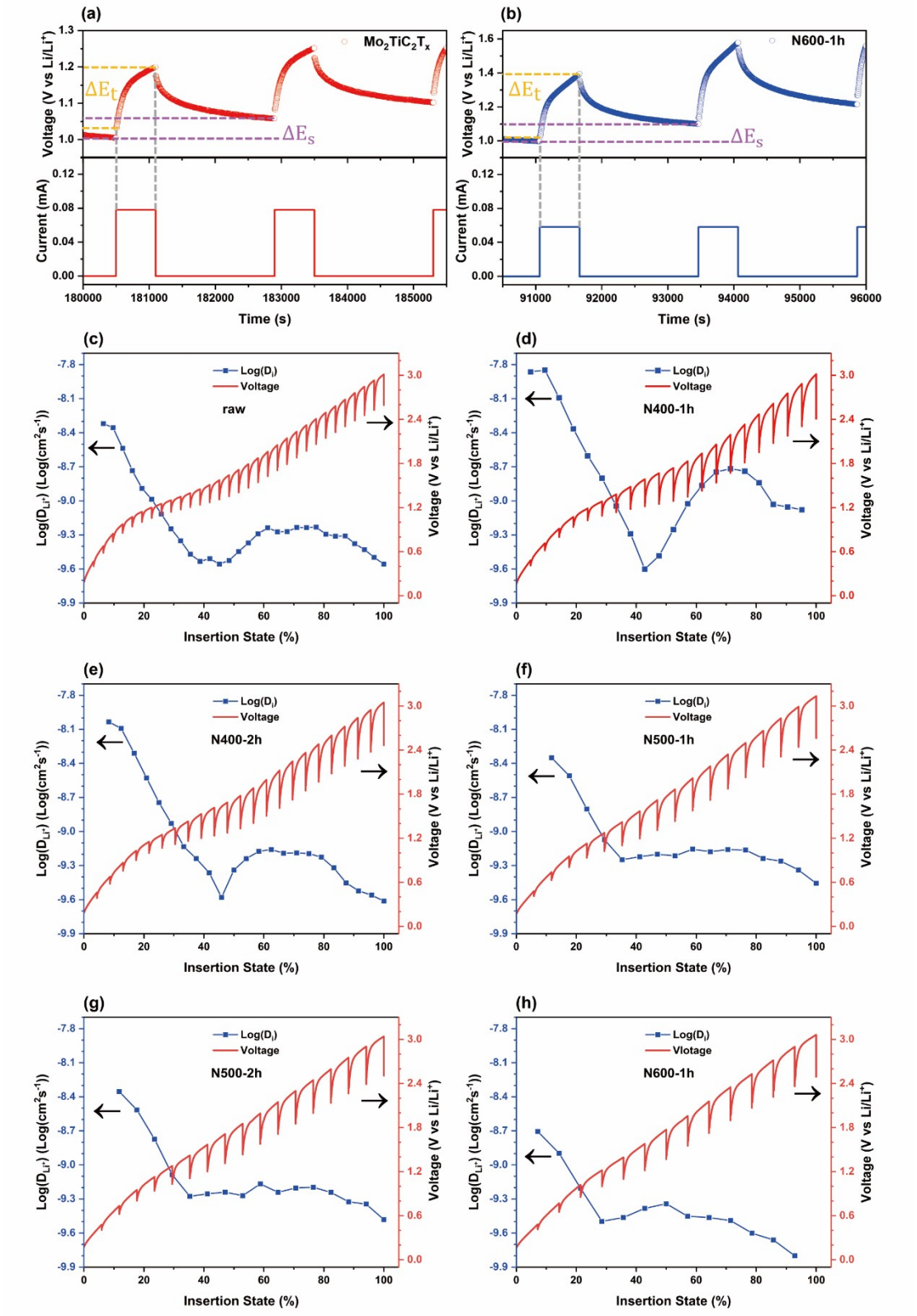

Figure S9. GITT voltage curve and current curve for (a) $Mo_2TiC_2T_x$, (b) N400-1h during the charge stage. The ΔE_t and ΔE_s values (Eqs. 9 in main text) are indicated. GITT curves and Li^+ diffusion coefficient of (c) $Mo_2TiC_2T_x$, (d) N400-1h, (e) N400-2h, (f) N500-1h, (g) N500-2h and (h) N600-1h.

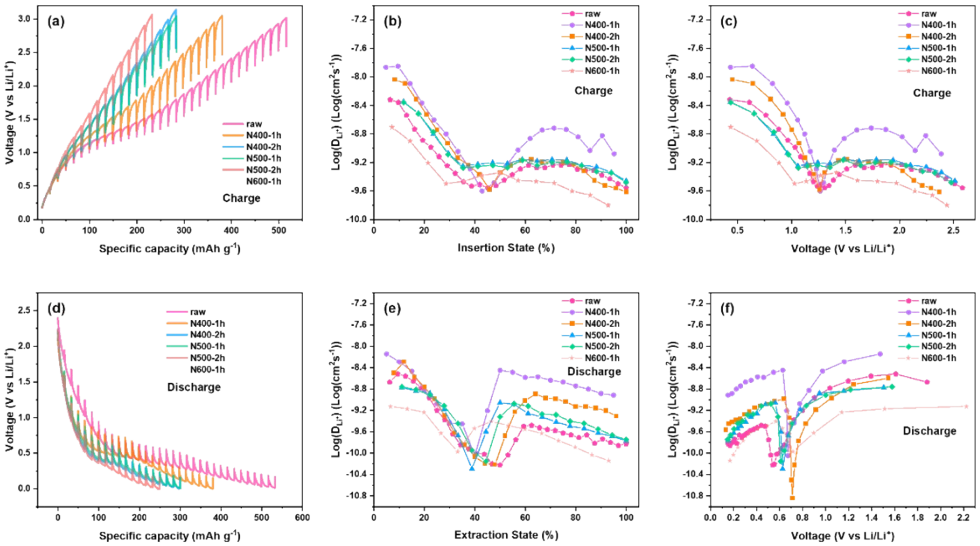

Figure S10. GITT voltage and specific capacity curve in (a) charge and (d) discharge process; GITT curve for (b) insertion and (e) extraction state; GITT voltage curve in (c) charge and (f) discharge process.

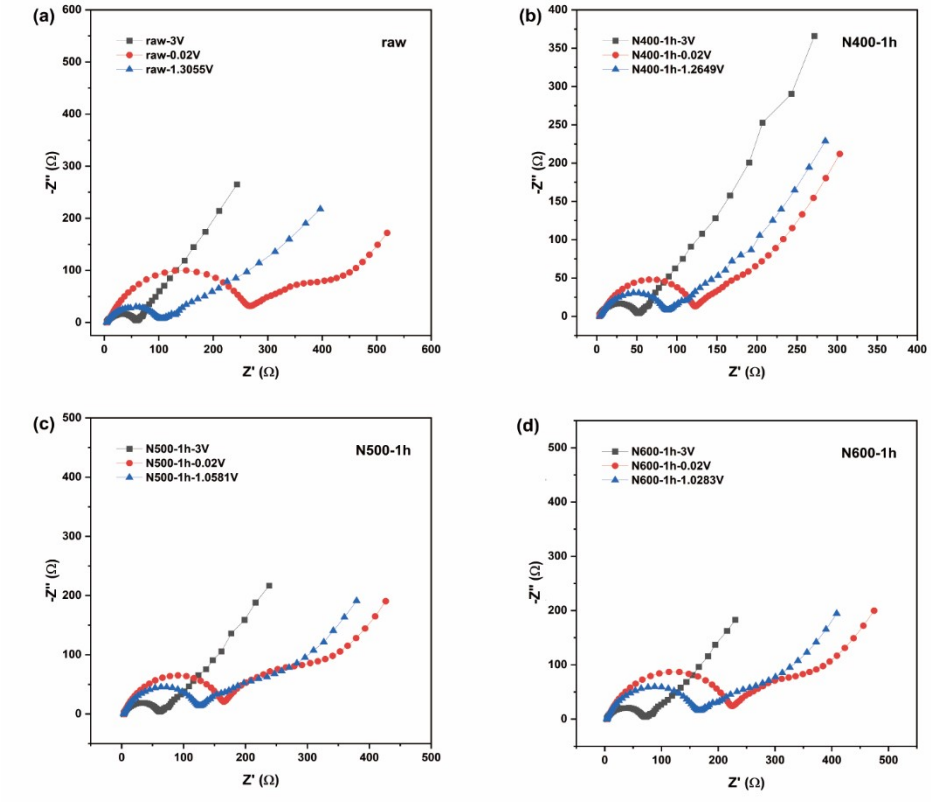

Figure S11. EIS at three points of voltage for sample (a)raw, (b)N400-1h, (c)N500-1h, (d)N600-1h.

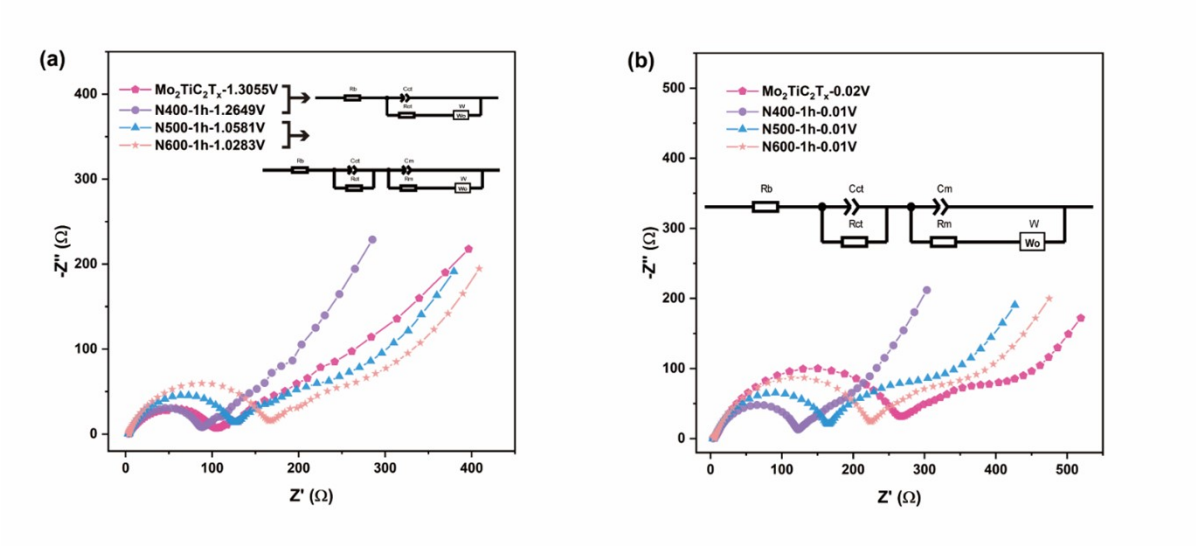

Figure S12. The EIS of raw and ammoniated $Mo_2TiC_2T_x$ MXenes at (a) the specific potential; (b) 0.01 V.

Table S15. Simulation results of the EIS spectra of $Mo_2TiC_2T_x$

Element	3 V		1.305 V		0.01 V	
	Values	Error (%)	Values	Error (%)	Values	Error (%)
R_b (Ω)	4.2	1.8	4.1	2.80	4.4	1.4
R_{ct} (Ω)	54.4	3.8	92.3	1.71	226.34	2.3
C_{ct} (F)	7.0E-05	2.1	4.3E-05	2.09	2.6E-05	1.0
W-R (Ω)	2.8	1.6	2.8	2.40	64.6	1.8
W-T (F)	0.013	2.4	5.6 E-04	5.26	0.21	2.3

Table S16. Simulation results of the EIS spectra of N400-1h

Element	3 V		1.265 V		0.01 V	
	Values	Error (%)	Values	Error (%)	Values	Error (%)
R_b (Ω)	3.0	2.0	3.8	1.5	3.6	2.5
R_{ct} (Ω)	39.6	2.0	77.7	1.6	110.3	2.4
C_{ct} (F)	4.7E-05	2.0	4.6E-05	1.4	4.9E-05	1.7
W-R (Ω)	5.5	1.6	2.1	1.5	1.3	2.5
W-T (F)	0.035	2.5	0.22	1.3	7.4	5.2

Table S17. Simulation results of the EIS spectra of N500-1h

Element	3 V		1.058 V		0.01 V	
	Values	Error (%)	Values	Error (%)	Values	Error (%)
R_b (Ω)	3.4	1.9	3.4	1.8	3.8	1.3
R_{ct} (Ω)	48.8	3.1	106.5	2.1	141.4	1.3
C_{ct} (F)	3.9E-05	1.9	2.8E-05	1.0	2.5E-05	1.1
R_m (Ω)	-	-	81.1	4.1	348.4	2.7
C_m (F)	-	-	5.4E-03	3.2	5.7E-03	3.0
W-R (Ω)	13.1	1.8	4.9	4.5	8.3	9.0
W-T (F)	0.11	3.2	0.081	9.4	2.5E-03	9.5

Table S18. Simulation results of the EIS spectra of N600-1h

Element	3 V		1.028 V		0.01 V	
	Values	Error (%)	Values	Error (%)	Values	Error (%)
R_b (Ω)	3.7	1.9	3.7	1.46	4.3	3.6
R_{ct} (Ω)	59.1	3.1	144.5	0.81	199.7	2.1
C_{ct} (F)	3.4E-05	1.9	2.2E-05	0.98	2.0E-05	1.1
R_m (Ω)	-	-	197.4	5.9	538.9	12.1
C_m (F)	-	-	4.6E-03	4.7	6.9E-03	3.5
W-R (Ω)	18.3	1.9	7.6	4.0	17.1	12.2
W-T (F)	0.18	3.7	0.062	7.4	0.32	12.8

Reference

[1] Asia Sarycheva and Yury Gogotsi, Raman Spectroscopy Analysis of the Structure and Surface Chemistry of $Ti_3C_2T_x$ MXene, Chem. Mater. 2020, 32, 8, 3480–3488.

[2] J. I. Langford and A. J. C. Wilson, Scherrer after sixty years: A survey and some new results in the determination of crystallite size, J. Appl. Crystallogr., 1978, 11, 102-113.

[3] Dongsheng Geng, Songlan Yang, Yong Zhang, Jinli Yang, Jian Liu, Ruying Li, Tsun-Kong Sham, Xueliang Sun, Siyu Ye and Shanna Knights, Nitrogen doping effects on the structure of graphene, Appl. Surf. Sci., 2011, 257, 9193-9198.

[4] Binoy K. Saikia, Rajani K. Boruah and Pradip K. Gogoi, A X-ray diffraction analysis on graphene layers of Assam coal, J. Chem. Sci., 2009, 121, 103-106.

[5] Joseph Halima, Kevin M. Cook, Per Eklund, Johanna Rosen, Michel W. Barsoum, XPS of cold pressed multilayered and freestanding delaminated 2D thin films of $Mo_2TiC_2T_z$ and $Mo_2Ti_2C_3T_z$ (MXenes), Applied Surface Science, 2019, 494, 1138-1147.

[6] Patrick Urbankowski, Babak Anasori, Kanit Hantanasirisakul, Long Yang, Lihua Zhang, Bernard Haines, Steven J. May, Simon J. L. Billinge and Yury Gogotsi, 2D molybdenum and vanadium nitrides synthesized by ammoniation of 2D transition metal carbides (MXenes), Nanoscale, 2017, 9, 17722.

[7] J. Moulder, W. Stickle, W. Sobol, K. D. Bomben, Handbook of x-ray photoelectron spectroscopy A Reference Book of Standard Spectra for Identification, Physical Electronics, 1995.

[8] V. Augustyn, J. Come, M.A. Lowe, J.W. Kim, P.L. Taberna, S.H. Tolbert, H.D. Abruna, P. Simon, B. Dunn, High-rate electrochemical energy storage through Li+ intercalation pseudocapacitance, Nat. Mater. 2013, 12, 518–522.

[9] Shchukarev A, Korolkov D. XPS Study of Group IA Carbonates. Open Chem. 2004, 2, 347-362.

[10] B. Brox, I. Olefjord. ESCA Studies of MoO_2 and MoO_3. Surface and Interface Analysis, 1988, 13, 3.

[11] Lu YC, Crumlin E. J, Veith G. M, et al. In Situ Ambient Oressure X-Ray Photoelectron Spectroscopy Studies of Lithium-Oxygen Redox Reactions. Sci. Rep. 2012, 2, 1-6.

[12] Oswald S. Binding Energy Referencing for XPS in Alkali Metal-Based Battery Materials Research (I): Basic Model Investigations. Appl. Surf. Sci. 2015, 351, 492-503.

[13] N. S. McIntyre, D. D. Johnston, L. L. Coatsworth, et al. X-ray photoelectron spectroscopic studies of thin film oxides of cobalt and molybdenum. Surface and Interface Analysis, 1990, 15, 265.

[14] Sanjines R., Wiemer C., Almeida J., et al. Valence band photoemission study of the Ti Mo N system. Thin Solid Films, 1996, 290-291, 334-338.